Available online at www.sciencedirect.com
ScienceDirect
Journal of Sound and Vibration 321 (2009) 115–136
JOURNAL OF SOUND AND VIBRATION
www.elsevier.com/locate/jsvi

The axial–torsional vibration of pretwisted beams

Kuang-Chen Liu, James Friend*, Leslie Yeo

MicroNanophysics Research Laboratory, Department of Mechanical Engineering, Monash University, Victoria 3800, Australia

Received 16 January 2007; received in revised form 10 July 2008; accepted 11 September 2008
Handling Editor: L.G. Tham
Available online 19 October 2008

Abstract

We investigate the coupled axial–torsional vibration of pretwisted beams. The equations of motion governing the extension, torsion, and cross-sectional warping of pretwisted beams are derived from Hamiltons principle, and the common assumptions used to simplify the equations are carefully examined through scaling analysis. Inconsistencies in previous works—such as the neglect of spatial and time derivatives of torsion in the Lagrangian functional—are remedied, giving rise to fourth-order terms in the equations of motion that are significant for higher harmonics. Furthermore, scaling analysis of the governing equations yields a set of objective criteria for checking the validity of the frequently misused assumption that the warping function under pretwist is locally identical to that of a prismatic beam; we show that this simplification is responsible for the common poor prediction of axial resonance frequencies for pretwisted beams.

1. Introduction

Pretwisted beams exhibit interesting coupling phenomena between extension, torsion and flexure, and have been the subject of extensive research due to their importance as models for aircraft and helicopter rotor blades [1]. More recently, a new application exploiting the beam's inherent axial–torsional coupling has also been demonstrated in the design of a piezoelectric ultrasonic motor with great miniaturization potential [2].

Due to the complex geometry of pretwisted beams, past researchers have developed a number of approximate theories. An early approach with mixed results was Chu's helical fiber assumption [3], where stresses are initially determined along and perpendicular to helical fibers of the beam's pretwist. While its predictions matched experimental results for thin-walled beams, it was nevertheless a flawed theory that predicted axial–torsional coupling where none is present (e.g. beams with circular cross-sections).

In recent years, warping function-based beam theories appear to have become widely accepted [1] since they overcome the shortcomings of the helical fiber assumption—correctly predicting that pretwist has no effect on beams with circular cross-sections. Representatives of the theory include the works of Rosen [4,5], Hodges [6], Krenk [7] on static axial–torsional coupling, and Rosen [1], Tsuiji [8] on the dynamic response.

*Corresponding author. Tel.: +61 3 9905 3551; fax: +61 3 9905 1825.
E-mail address: james.friend@eng.monash.edu.au (J. Friend).
URL: http://mnrl.monash.edu.au (J. Friend).

0022-460X/$ - see front matter © 2008 Elsevier Ltd. All rights reserved.
doi:10.1016/j.jsv.2008.09.016

The warping function theories are based on semi-inverse and variational methods. The semi-inverse method was proposed by Saint-Venant for solving the elastic deformation of prismatic rods under resultant end loads, force F_T and moment F_M [9,10]. The method simplifies the governing equations of the problem by making assumptions about the functional form of the displacement field based on 'physical insights'. Accordingly, the correctness and complexity of the resulting equations depend crucially on the initial choice of the compatible displacement field. Two common assumptions are made for the coupled extension–torsion problem: first, that deformation parallel to the cross-sections is negligible, and second, that axial deformation consists of bulk displacement $\bar{u}$ and cross-sectional warping ψ. For example, the displacement field used by Rosen [5] (and Tsuiji [8] if we neglect bending) is

$$u(x,y,z,t) = \bar{u}(x,t) + \phi'(x,t)\psi(x,y,z), \tag{1a}$$

$$v(x,y,z,t) = y[\cos\phi(x,t) - 1] - z\sin\phi(x,t), \tag{1b}$$

$$w(x,y,z,t) = y\sin\phi(x,t) + z[\cos\phi(x,t) - 1], \tag{1c}$$

where u, v, w are, respectively, the displacement components in the x, y, z directions, and ϕ represents the angle of elastic rotation additional to the pretwist angle β (see Fig. 1). Following standard convention, primes and over dots denote differentiation with respect to x and t.

Note that the cross-sectional warping ψ is the *single* term that accounts for the axial–torsional coupling of pretwisted beams in these theories. Given the importance of the warping function in the coupling between extension and torsion, it is surprising that no one, to our knowledge, has derived the governing equations for the warping function of *pretwisted beams*. Most researchers simply assume that it has the same form as the warping function of *prismatic beams* expressed in the local coordinates (η, ζ).

Although Krenk [11] showed that the prismatic beam warping function is the leading term in the axial–torsional coupling, the result was derived from an asymptotic solution to the three-dimensional equations of elasticity. This means that the assumption is valid only for beams with small pretwist, and it is unclear, quantitatively, at what limit the approximation fails.

The equations of motion for the axial–torsional vibration of pretwisted beams derived by Rosen [1] have the following form:

$$\begin{aligned} a_1\bar{u}'' + a_2\phi'' &= \ddot{\bar{u}}, \\ b_1\bar{u}'' + b_2\phi'' &= \ddot{\phi}, \end{aligned} \tag{2}$$

which is the same as those derived by Tsuiji [8], and Curti and Risitano [12] except for slight differences in the coefficients. While the torsional resonance frequencies predicted by Eqs. (2) matches results of finite-element analysis (FEA) at low pretwist, a careful examination of Rosen's work shows, however, that Eqs. (2) are physically inconsistent with the assumptions used in its derivation.

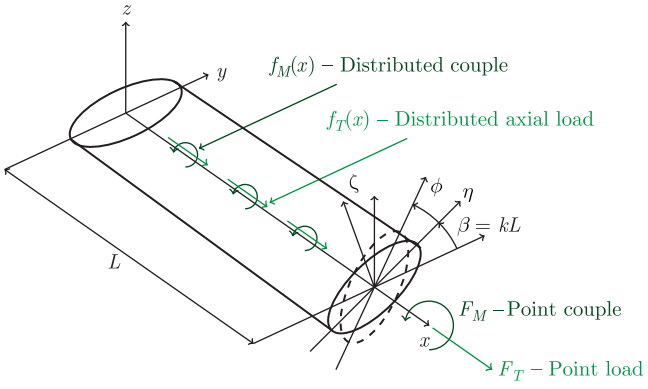

Fig. 1. The coordinate systems used to describe the pretwisted beam, and the external forces and moments acting on the beam.

Rosen [1] derived Eqs. (2) by adding inertia terms to the linearized version of the static load–deformation relations he obtained in Ref. [5]. This is equivalent to forming the Lagrangian functional by adding kinetic energy terms to the potential energy function in Ref. [5] and applying Hamilton's principle, noting the fact that he neglects the mixed derivative term in the kinetic energy, $\psi\dot{\phi}'$, and assumes that torsion is uniform $\phi''=0$. The uniform torsion assumption—which simplifies the potential energy function considerably—is only valid for static cases, however, Rosen carried it into the dynamic case and allowed ϕ'' to 'slip' back into Eq. (2). Examining these assumptions further, solutions of equations (2) imply that

$$\phi(x)\sim\Phi\cos(\lambda x)e^{i\omega t},$$

$$|\phi''|\sim\lambda^2\Phi \quad \text{and} \quad |\dot{\phi}'|\sim\lambda\omega\Phi, \tag{3}$$

where $\lambda\sim1/L$ and $\omega\sim10^4/L$ for metal beams of length L. Thus the neglected terms are, in fact, of similar or larger magnitude than the retained terms when $L<1$.

The present work is divided into three sections. In the first section, we provide a rigorous derivation of the equations governing the axial–torsional coupling of pretwisted beams. The semi-inverse method and Eqs. (1) remain the starting point; however, we retain the mixed derivative term $\psi\dot{\phi}'$ in the velocity field and we do not assume torsion to be uniform. This results in fourth-order terms with very small coefficients in the new equations of motion, thus explaining the apparent success of Eqs. (2) in predicting low harmonic frequencies at low pretwist. Most importantly, we derive the governing equations for the cross-sectional warping of pretwisted beams by treating ψ as an unknown dependent function in the application of Hamilton's principle. Scaling analysis is then used to obtain an objective set of criteria to quantify the limits under which prismatic beam warping function and other simplifying assumptions may be consistently applied on a physically justifiable basis.

In the second section, we solve the new equations of motion and compare its resonance frequency predictions with FEA results. Two significant results are drawn from the comparison. First, the criteria successfully predict geometries for which significant error will appear; it gives clear guidelines as to when the warping function simplification is valid. Second, the misuse of the prismatic warping function is shown to be the leading cause for the poor prediction of axial resonance frequencies by warping function-based beam theories.

Note that we ensure bending is uncoupled from torsion and extension by restricting the geometry of the beam such that the centroid and shear centre coincide with the axis of pretwist [5,13,14]. Furthermore, the beam begins stress-free in the pretwisted configuration; the axial–torsional coupling investigated in this paper are those present due to the geometry alone.

2. Equations of motion

The equations of motion are derived using Hamilton's principle:

$$\delta\int_{t_1}^{t_2}(T+W_{\text{ext}}-U)\,dt=0, \tag{4}$$

where T is the kinetic energy, W_{ext} is the work done by external forces, U is the strain energy, and δ is the delta-operator for the first variation. Note that the deformed state of the pretwisted beam can be described using two coordinate systems (CS): an orthogonal CS (x,y,z), and a rotating CS (x,η,ζ), where η and ζ rotate with the pretwist angle $\beta(x)$ (see Fig. 1). In this section the orthogonal CS is used since it allows simpler derivation of the equation of motion. Later a switch is made to the rotating CS where simpler boundary conditions can be used when various sectional integrals involving the warping function need to be evaluated.

2.1. Describing the motion and the deformation

In order to express the strain energy in terms of the displacement field, Green's strain-displacement relation is used:

$$\varepsilon_{ij}=\frac{1}{2}\left[\frac{\partial u_j}{\partial x_i}+\frac{\partial u_i}{\partial x_j}+\frac{\partial u_\alpha}{\partial x_i}\frac{\partial u_\alpha}{\partial x_j}\right]. \tag{5}$$

The resulting strain components are

$$\varepsilon_{xx} = \frac{\partial u}{\partial x} + \frac{1}{2}\left[\underline{\left(\frac{\partial u}{\partial x}\right)^2} + \underline{\underline{r^2\theta^2}}\right], \tag{6a}$$

$$\varepsilon_{xy} = \frac{1}{2}\theta\left[\frac{\partial \psi}{\partial y}\left(1 + \underline{\frac{\partial u}{\partial x}}\right) - z\right], \quad \varepsilon_{xz} = \frac{1}{2}\theta\left[\frac{\partial \psi}{\partial z}\left(1 + \underline{\frac{\partial u}{\partial x}}\right) + y\right], \tag{6b}$$

$$\varepsilon_{yy} = \underline{\underline{\frac{1}{2}\theta^2\left[\frac{\partial \psi}{\partial y}\right]^2}}, \quad \varepsilon_{yz} = \underline{\underline{\frac{1}{2}\theta^2\left[\frac{\partial \psi}{\partial y}\frac{\partial \psi}{\partial z}\right]}}, \quad \varepsilon_{zz} = \underline{\underline{\frac{1}{2}\theta^2\left[\frac{\partial \psi}{\partial z}\right]^2}}, \tag{6c}$$

where

$$\frac{\partial u}{\partial x} = \bar{\varepsilon}_{xx} + \theta\frac{\partial \psi}{\partial x} + \frac{\partial \theta}{\partial x}\psi,$$

$$\bar{\varepsilon}_{xx} = \frac{\partial \bar{u}}{\partial x}, \quad \theta = \frac{\partial \phi}{\partial x}, \quad r^2 = z^2 + y^2. \tag{7}$$

To express the kinetic energy in terms of the displacement field, the velocity vector $\dot{\mathbf{R}}$ of each point in the beam is given by

$$\begin{aligned}\dot{\mathbf{R}} &= \dot{\mathbf{u}} = (\dot{u})\hat{e}_x + (\dot{v})\hat{e}_y + (\dot{w})\hat{e}_z \\ &= (\dot{\bar{u}} + \dot{\theta}\psi)\hat{e}_x + \dot{\phi}(-y\sin\phi - z\cos\phi)\hat{e}_y + \dot{\phi}(y\cos\phi - z\sin\phi)\hat{e}_z \\ &= (\dot{\bar{u}} + \dot{\theta}\psi)\hat{e}_x + r\dot{\phi}[-(\sin\phi)\hat{e}_r + (\cos\phi)\hat{e}_\phi],\end{aligned} \tag{8}$$

where the cartesian unit vectors $(\hat{e}_x, \hat{e}_y, \hat{e}_z)$ are transformed to cylindrical unit vectors $(\hat{e}_x, \hat{e}_r, \hat{e}_\phi)$ for compactness. The relationship between cartesian and cylindrical unit vectors is

$$\hat{e}_r = \frac{1}{r}(y\hat{e}_y + z\hat{e}_z) \quad \text{and} \quad \hat{e}_\phi = \frac{1}{r}(-z\hat{e}_y + y\hat{e}_z). \tag{9}$$

2.2. Scaling and order of magnitude analysis

There is a need to simplify Eqs. (6); when fully expanded, Eq. (6a) has 11 terms, which in turn contributes 66 terms to the strain energy. We therefore scale the governing equations in order to carry out an order of magnitude analysis such that insignificant terms can be neglected on a physically justifiable and consistent basis. By dividing each of the three dependent variables $(\bar{u}, \phi, \psi)$ and the four independent variables (x, y, z, t) by an appropriate characteristic length scale (denoted with subscript c), the following non-dimensionalized variables (denoted with a subscript s) are obtained:

$$\bar{u}_s = \frac{\bar{u}}{\bar{u}_c}, \quad \phi_s = \frac{\phi}{\phi_c}, \quad \psi_s = \frac{\psi}{\psi_c} = \frac{\psi}{r_c^2}, \quad x_s = \frac{x}{x_c} = \frac{x}{L},$$

$$y_s = \frac{y}{r_c}, \quad z_s = \frac{z}{r_c}, \quad t_s = \frac{t}{t_c} = \frac{t}{L}\sqrt{\frac{E}{\rho}}, \tag{10}$$

where $x_c = L$ is the beam length and $y_c = z_c = r_c$ is the radius of the circle inscribing the beam cross-section; $t_c = L\sqrt{\rho/E}$ is the time scale of the axial resonance frequency of the prismatic beam (chosen as a reference), ρ and E are, respectively, density and modulus of elasticity. The scale for the warping function, $\psi_c = r_c^2$ is estimated from the Saint-Venant warping function ψ_{Ellipse} of a prismatic elliptical beam [15]; similar estimates may be obtained for other cross-sections,

$$\psi_{\text{Ellipse}} = -\frac{a^2 - b^2}{a^2 + b^2}yz = -\frac{1 - (b/a)^2}{1 + (b/a)^2}yz = -Byz, \tag{11}$$

where a and b are the semi-major and semi-minor axes, and $B \in (-1, 1)$ is a dimensionless coefficient. Substituting Eqs. (10) and (11) into $\psi_c = \psi/\psi_s$ provides the following estimate for ψ_c:

$$\psi_c = \frac{\psi}{\psi_s} = \frac{-B(r_c y_s)(r_c z_s)}{-B y_s z_s} = r_c^2. \tag{12}$$

The definitions for the characteristic deformations $(\bar{u}_c, \phi_c)$ are chosen at a later stage to simplify the non-dimensional form of the equations of motion (see Section 3.1). They are shown here for completeness;

$$\bar{u}_c = \frac{f_{T0} L^2}{EA} \quad \text{and} \quad \phi_c = \frac{f_{T0} L^3}{E\sqrt{K_0 A}}, \tag{13}$$

where (f_{T0}, f_{M0}) are the characteristic amplitudes of the distributed axial and torsional loads (f_T, f_M). Note the use of f_{T0} for ϕ_c is intentional.

Applying the change of variables in Eq. (10)–(6), the terms contributing to strain may be separated into four classes by their non-dimensional coefficients (NDCs) as shown in Table 1. Note that the NDCs are obtained by dividing the dimensional coefficient by $\phi_c r_c/L$, and the subscript comma notation denotes partial differentiation:

$$\psi_{,y} = \frac{\partial \psi}{\partial y}, \tag{14}$$

and

$$\psi_{,z} = \frac{\partial \psi}{\partial z}. \tag{15}$$

A comparison of the relative magnitude of the NDCs shows that if the characteristic axial strain $\varepsilon_c = \bar{u}_c/L$ and the characteristic shear strain $\gamma_c = \phi_c r_c/L$ are small (i.e. $\varepsilon_c \ll 1$ and $\gamma_c \ll 1$) then the underlined terms in Eqs. (6) and Class 4 terms in Table 1 (doubly underlined in Eqs. (6)) can be ignored, thus simplifying the strain components to

$$\varepsilon_{xx} = \bar{\varepsilon}_{xx} + \theta \frac{\partial \psi}{\partial x} + \frac{\partial \theta}{\partial x}\psi, \tag{16a}$$

$$\varepsilon_{xy} = \frac{1}{2}\theta\left[\frac{\partial \psi}{\partial y} - z\right], \quad \varepsilon_{xz} = \frac{1}{2}\theta\left[\frac{\partial \psi}{\partial z} + y\right], \tag{16b}$$

$$\varepsilon_{yy} = \varepsilon_{yz} = \varepsilon_{zz} = 0. \tag{16c}$$

For example, an aluminium beam ($E = 71$ MPa, $G \simeq 27$ GPa, $\tau_{\text{yield}} \simeq 250$ MPa) with an elliptical cross-section satisfies the first condition in the elastic region ($\varepsilon_{\max} = 9.3 \times 10^{-3}$). Using Saint-Venant's theory of torsion for

Table 1
Classification of strain components by their non-dimensional coefficients (NDCs)

Class	Terms	Coefficients	NDC
1	$\frac{\partial \bar{u}}{\partial x}$	$\frac{\bar{u}_c}{L}$	$\frac{\bar{u}_c}{\phi_c r_c}$
2	$\theta\frac{\partial \psi}{\partial x}, \frac{\partial \theta}{\partial x}\psi$	$\frac{\phi_c r_c^2}{L^2}$	$\frac{r_c}{L}$
3	$\frac{1}{2}\theta\psi_{,y}, \frac{1}{2}\theta\psi_{,z}$, $\frac{1}{2}\theta z, \frac{1}{2}\theta y$	$\frac{1}{2}\frac{\phi_c r_c}{L}$	$\frac{1}{2}$
4	$\frac{1}{2}r^2\theta^2, \frac{1}{2}\theta^2\psi_{,y}^2$, $\frac{1}{2}\theta^2\psi_{,y}\psi_{,z}, \frac{1}{2}\theta^2\psi_{,z}^2$,	$\frac{1}{2}\frac{\phi_c^2 r_c^2}{L^2}$	$\frac{1}{2}\frac{\phi_c r_c}{L}$

prismatic beams [15],

$$\tau_{\max} = \frac{2Ga^2b}{a^2+b^2}\frac{\phi_c}{L} \Rightarrow \frac{\phi_c r_c}{L} = \frac{\tau_{\max}}{2G}\left(\frac{a}{b}+\frac{b}{a}\right), \tag{17}$$

and noting that $r_c = a$ (the radius of the inscribing circle), it can be estimated that $\gamma_c = \phi_c r_c/L < 0.05$ when the ellipse aspect ratio $b/a > 0.1$. This implies that Eqs. (16) may not be valid for extremely thin cross-sections. Note that the same strain components are obtained if an infinitesimal strain–displacement relation is used and the elastic rotation ϕ is limited to small angles (e.g. $\phi < 8^\circ$ for 1% error from the trigonometric functions in Eqs. (1)).

2.3. Strain energy, kinetic energy and applied work

The strain energy function is determined from the simplified strain components in Eqs. (16) and the constitutive law for elastic isotropic materials. Since $\varepsilon_{yy} = \varepsilon_{zz} = \varepsilon_{yz} = 0$, the constitutive law is given by

$$\tau_{xx} = E\varepsilon_{xx}, \quad \tau_{xy} = 2G\varepsilon_{xy}, \quad \tau_{xz} = 2G\varepsilon_{xz}. \tag{18}$$

The strain energy is thus

$$U = \iiint_V \frac{1}{2}E\varepsilon_{xx}^2 + 2G(\varepsilon_{xy}^2 + \varepsilon_{xz}^2)\,\mathrm{d}V. \tag{19}$$

Substituting Eqs. (16) into Eq. (19), the strain energy (in terms of the displacement field) is found to be

$$\begin{aligned} U = \iiint_V &\frac{1}{2}E(\bar{\varepsilon}_{xx}^2 + (\theta'\psi)^2 + (\theta\psi')^2) + E(\bar{\varepsilon}_{xx}\theta'\psi + \bar{\varepsilon}_{xx}\theta\psi' + \theta'\theta\psi'\psi) \\ &+ \frac{1}{2}G\theta^2\left[\left(\frac{\partial\psi}{\partial y} - z\right)^2 + \left(\frac{\partial\psi}{\partial z} + y\right)^2\right]\mathrm{d}V. \end{aligned} \tag{20}$$

The kinetic energy is given by

$$T = \iiint_V \frac{1}{2}\rho|\dot{\mathbf{R}}|^2\,\mathrm{d}V, \tag{21}$$

which, upon the substitution of $\dot{\mathbf{R}}$ from Eq. (8) results in

$$T = \iiint_V \frac{1}{2}\rho[\dot{\bar{u}}^2 + 2\dot{\bar{u}}\dot{\theta}\psi + \dot{\theta}^2\psi^2 + r^2\dot{\phi}^2]\,\mathrm{d}V. \tag{22}$$

The work done by external forces is

$$\begin{aligned} W_{\text{ext}} &= \int_{x=0}^{L} F_T\bar{\varepsilon}_{xx} + F_M\theta + f_T\bar{u} + f_M\phi\,\mathrm{d}x \\ &= \iiint_V \frac{\mathrm{d}F_T}{\mathrm{d}A}\bar{\varepsilon}_{xx} + \frac{\mathrm{d}F_M}{\mathrm{d}A}\theta + \frac{\mathrm{d}f_T}{\mathrm{d}A}\bar{u} + \frac{\mathrm{d}f_M}{\mathrm{d}A}\phi\,\mathrm{d}V, \end{aligned} \tag{23}$$

where the force $F_T(t)$ and moment $F_M(t)$ are applied at the ends of the beam, and the tensile force $f_T(x,t)$ and moment $f_M(x,t)$ are distributed along the axis of the beam.

With the applied work, kinetic and elastic energies now expressed in terms of three unknown functions $\bar{u}, \phi$, and ψ, Hamilton's principle may be applied to derive the equations of motion (see Appendix A for details). Since there are three dependent variables, there are three governing equations:

$$\frac{\mathrm{d}f_T}{\mathrm{d}A} + E\frac{\partial}{\partial x}(\bar{\varepsilon}_{xx} + \theta'\psi + \theta\psi') = \rho\frac{\partial}{\partial t}(\dot{\bar{u}} + \dot{\theta}\psi), \tag{24a}$$

$$\frac{\mathrm{d}f_M}{\mathrm{d}A}+E\frac{\partial}{\partial x}(\theta\psi'^2+\bar{\varepsilon}_{xx}\psi'+\theta'\psi\psi')+G\frac{\partial}{\partial x}[\theta((\psi_{,y}-z)^2+(\psi_{,z}+y)^2)]$$
$$-E\frac{\partial^2}{\partial x^2}(\theta'\psi^2+\bar{\varepsilon}_{xx}\psi+\theta\psi\psi')=\rho\frac{\partial}{\partial t}(r^2\dot{\phi})-\rho\frac{\partial^2}{\partial x\partial t}(\dot{\bar{u}}\psi+\dot{\theta}\psi^2), \tag{24b}$$

$$\rho(\dot{\theta}\dot{\bar{u}}+\dot{\theta}^2\psi)-E(\theta'^2\psi+\bar{\varepsilon}_{xx}\theta'+\theta\theta'\psi')+E\frac{\partial}{\partial x}(\theta^2\psi'+\bar{\varepsilon}_{xx}\theta+\theta\theta'\psi)+G\theta^2\underline{\left[\frac{\partial}{\partial y}(\psi_{,y}-z)+\frac{\partial}{\partial z}(\psi_{,z}+y)\right]}=0, \tag{24c}$$

where the natural boundary conditions over the entire surface of the beam are

$$\oint\!\!\!\oint\left(-E(\bar{\varepsilon}_{xx}+\theta'\psi+\theta\psi')+\frac{\mathrm{d}F_T}{\mathrm{d}A}\right)a_{nx}\,\mathrm{d}A=0, \tag{25a}$$

$$\oint\!\!\!\oint\left(E(\psi\psi''\theta+2\psi\psi'\theta'+\psi^2\theta''+\psi\bar{u}'')-\rho(\psi\ddot{\bar{u}}+\psi^2\ddot{\theta})-G[(\psi_{,y}-z)^2+(\psi_{,z}+y)^2]\theta+\frac{\mathrm{d}F_M}{\mathrm{d}A}\right)a_{nx}\,\mathrm{d}A=0, \tag{25b}$$

$$\oint\!\!\!\oint-E(\psi^2\theta'+\psi\bar{u}'+\psi\psi'\theta)a_{nx}\,\mathrm{d}A=0, \tag{25c}$$

$$\oint\!\!\!\oint E(\theta^2\psi'+\bar{\varepsilon}_{xx}\theta+\theta\theta'\psi)a_{nx}+G\theta^2\underline{[(\psi_{,y}-z)a_{ny}+(\psi_{,z}+y)a_{nz}]}\,\mathrm{d}A=0, \tag{25d}$$

and a_{nx}, a_{ny}, a_{nz} are components of the normal vectors on the surface of the beam. The initial conditions are given at the end of Appendix A.

2.4. Simplification of the warping function

The full governing equations for extension, torsion and cross-sectional warping of pretwisted beams are fully three-dimensional, coupled, and nonlinear. To simplify the problem, we note that the underlined terms in Eqs. (24c) and (25d) are the governing equations for the Saint-Venant warping function of a prismatic bar. To determine the conditions under which the extra terms may be neglected for pretwisted beams, Eqs. (24c) and (25d) are scaled by substituting the change of variables defined in Eqs. (10). The terms in the resulting equations may be separated into six classes by their NDCs (see Table 2): Classes 5–7 are terms from Eq. (24c), non-dimensionalized with respect to $G\phi_c^2/L^2$; and Classes 8–10 are terms from Eq. (25d), non-dimensionalized with respect to $\mathbb{X}$, where

$$\mathbb{X}=G\frac{\phi_c^2 r_c}{L^2}a_{nr}, \tag{26}$$

and

$$a_{nr}=\sqrt{a_{ny}^2+a_{nz}^2}. \tag{27}$$

If NDC 5, 6, 8 and 9 are small relative to unity (in other words, small relative to NDC 7 and 10), then we can simplify Eqs. (24c) and (25d) to the following:

$$\nabla^2\psi=0, \tag{28a}$$

$$\left(\frac{\partial\psi}{\partial y}-z\right)a_{ny}+\left(\frac{\partial\psi}{\partial z}+y\right)a_{nz}=0\quad\text{along the boundary of the cross-section,} \tag{28b}$$

which are the governing equations of the warping function for prismatic beams. In order to determine the conditions under which NDC 5, 6, 8 and 9 are small, we note that the NDCs can be expressed in terms of four non-dimensional parameters: the slenderness ratio SL, the amplitude ratio AP, the tilt ratio of surface normal

Table 2
Classification of the components of Eqs. (24c) and (25d) by their non-dimensional coefficient (NDCs)

Class	Terms	Coefficients	NDC
5	$\rho\dot{\theta}\dot{\bar{u}}$,	$\rho\frac{\phi_c\bar{u}_c}{Lt_c^2}$,	
	$E\bar{\varepsilon}_{xx}\theta'$, $E\frac{\partial}{\partial x}(\bar{\varepsilon}_{xx}\theta)$	$E\frac{\phi_c\bar{u}_c}{\partial L^3}$	$\frac{E\ \bar{u}_c\ r_c}{G\phi_c r_c L} \equiv \frac{E\mathrm{SL}}{G\mathrm{AP}}$
6	$\rho\dot{\theta}^2\psi$,	$\rho\frac{\phi_c^2 r_c^2}{L^2 t_c^2}$,	
	$E\theta'^2\psi$, $E\theta\theta'\psi'$, $E\frac{\partial}{\partial x}(\theta^2\psi')$, $E\frac{\partial}{\partial x}(\theta\theta'\psi)$,	$E\frac{\phi_c^2 r_c^2}{L^4}$	$\frac{E\,r_c^2}{GL^2} \equiv \frac{E}{G}\mathrm{SL}^2$
7	$G\theta^2\frac{\partial^2\psi}{\partial y^2}$, $G\theta^2\frac{\partial^2\psi}{\partial z^2}$	$G\frac{\phi_c^2}{L^2}$	1
8	$E\bar{\varepsilon}_{xx}\theta a_{nx}$	$E\frac{\phi_c\bar{u}_c}{L^2}a_{nx}$	$\frac{E\ \bar{u}_c\ a_{nx}}{G\phi_c r_c a_{nr}} \equiv \frac{E\mathrm{TR}}{G\mathrm{AP}}$
9	$E\theta^2\psi' a_{nx}$, $E\theta\theta'\psi a_{nx}$	$E\frac{\phi_c^2 r_c^2}{L^3}a_{nx}$	$\frac{E r_c a_{nx}}{GL a_{nr}} \equiv \frac{E}{G} \times \mathrm{SL} \times \mathrm{TR}$
10	$G\theta^2(\psi_{,y} - z)a_{ny}$,	$G\frac{\phi_c^2 r_c}{L^2}a_{ny}$,	$\frac{a_{ny}}{a_{nr}}$
	$G\theta^2(\psi_{,z} + y)a_{nz}$,	$G\frac{\phi_c^2 r_c}{L^2}a_{nz}$,	$\frac{a_{nz}}{a_{nr}}$

vectors TR, and Poisson's ratio v:

$$\mathrm{SL} = \frac{r_c}{L}, \quad \mathrm{AP} = \frac{\phi_c r_c}{\bar{u}_c}, \quad \mathrm{TR} = \frac{a_{nx}}{a_{nr}}, \quad \frac{G}{E} = \frac{1}{2(1+v)}. \tag{29}$$

Note that the tilt ratio is directly related to the rate of pretwist k; for a beam with rectangular cross-section of width a and height b ($a>b$), the maximum tilt ratio is given by

$$\mathrm{TR}_{\max} = \frac{ka}{2} = \frac{kr_c}{\sqrt{1+\mathrm{AR}^2}}, \tag{30}$$

where $\mathrm{AR} = b/a$ is the cross-section aspect ratio, and $kr_c = r_c\beta/L = \tan(\alpha)$ can be interpreted as a non-dimensional rate of pretwist related to the helix angle α (formed between the helix generated by the vertices at r_c and the beam axis). For a general procedure to determine the tilt ratio of a uniformly twisted beam see Appendix B.

With the exception of the amplitude ratio (AP), the magnitude of the NDCs depends purely on the geometry (SL, TR) and the material property (v) of the beam. If we let ε be a small number, the four inequalities NDC$<\varepsilon$ can be used as criteria for checking when NDC 5, 6, 8, 8 are small, in other words, the applicability of the simplified warping function of Eq. (28b). In Fig. 2, the region in the parameters space (SL, TR, AP) satisfying $\varepsilon = 0.1$ and 0.05 are shaded, respectively, in light grey and dark grey (note that we fix Poisson's ratio at 0.3 since it approximates the behaviour of a wide range of materials). The physical interpretation of Fig. 2 regarding the conditions for applying Eq. (28b) is as follows: the flat cap on the slenderness ratio implies that the beam should be slender; the variable threshold on the amplitude ratio implies that the torsional deformation should be dominant over the axial deformation; finally, the limit on the allowable tilt ratio sets a maximum on the allowable pretwist.

While Eq. (28b) appears identical to the governing equations for Saint-Venant's warping function of prismatic bars, there is a subtle difference in the solution for ψ. In the present problem, the bar is pretwisted and hence the components of the surface normal vectors (a_{ny}, a_{nz}) are not constant along the beam. By applying a coordinate transformation from the orthogonal CS (x, y, z) to the rotating CS (x, η, ζ), Eq. (28b) is

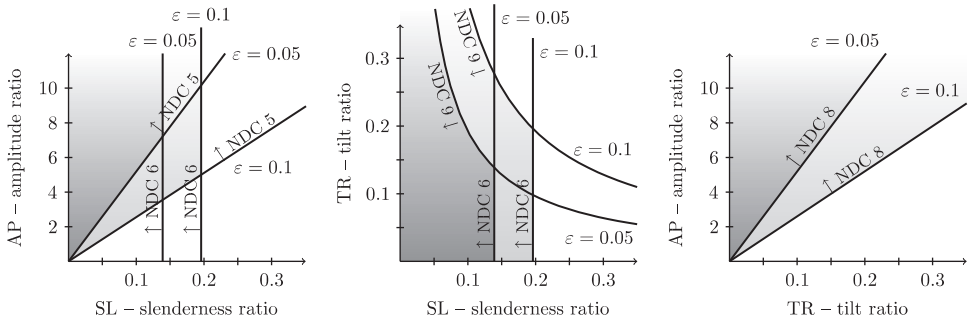

Fig. 2. The region in the parameter space (SL, TR, AP) where NDC 5, 6, 8 and 9 are less than ε, representing the criteria under which the simplified warping function equation (28b) is valid. The region where $\varepsilon = 0.1$ is shaded in light grey, and the region where $\varepsilon = 0.05$ is shaded in dark grey.

shown to be

$$\nabla^2\psi = 0, \tag{31a}$$

$$\left(\frac{\partial\psi}{\partial\eta} - \zeta\right)a_{n\eta} + \left(\frac{\partial\psi}{\partial\zeta} + \eta\right)a_{n\zeta} = 0 \quad \text{along the boundary of the cross-section,} \tag{31b}$$

where $(a_{n\eta}, a_{n\zeta})$ are now constant. Thus when the NDC$<\varepsilon$ criteria are satisfied, the warping functions of prismatic bars can be applied to pretwisted beams through a simple modification: replacing (y, z) by (η, ζ).

2.5. The simplified equations of motion

The above results on the warping function allow substantial simplification of the governing equations: they become linear and may be integrated over the cross-section to reduce the governing equations to a one-dimensional form. While the modification of the prismatic warping function for use in pretwisted beams is not new, the scaling analysis presented in Section 2.4, culminating in NDC 5, 6, 8, 9 and the NDC$<\varepsilon$ criteria shown in Fig. 2, forms the central result of this paper. The criteria allows the prediction of conditions under which the commonly used simplification of the warping function fails. The last point is important in applications that involve beams with high rates of pretwist. In Section 3.3 we demonstrate the utility of this result in highlighting beam geometries that falls outside the region where Eqs. (31) is valid.

Note that if the reduction of the governing equations to one-dimensional form is attempted by the sectional integration of Eqs. (24) and (25), we obtain a set of physically inconsistent equations,

$$EA\frac{\partial^2\bar{u}}{\partial x^2} + \underline{2ES_1}\frac{\partial^2\phi}{\partial x^2} = \rho A\frac{\partial^2\bar{u}}{\partial t^2}, \tag{32a}$$

$$\underline{-ES_1}\frac{\partial^2\bar{u}}{\partial x^2} + (GJ_s - \underline{2EK_1} - \underline{3D_{02}})\frac{\partial^2\phi}{\partial x^2} - EK_0\frac{\partial^4\phi}{\partial x^4} = \rho I_p\frac{\partial^2\phi}{\partial t^2} - \rho S_1\ddot{\bar{u}} - \rho K_0\frac{\partial^4\phi}{\partial t^2 x^2}. \tag{32b}$$

There are two major objections to Eqs. (32). First, the Maxwell–Betti reciprocal theorem [15,16], which is satisfied by all linearly elastic structures, states that the stiffness coefficients are symmetric and thus the terms with a single underline in Eq. (32) should be equal. Second, K_1 and D_{02} are positive and increasing functions of pretwist, which means the terms of Eq. (32) in parentheses predict a fall in torsional stiffness as pretwist is increased; however, experimental results [1] and FEA (see Section 3.2) show that the torsional stiffness and resonance frequency should rise.

The appropriate places to perform the sectional integrations are on the energy–displacement field relations equations (20)–(23). This eliminates ψ as an unknown dependent variable and gives the following governing

equations:

$$f_T + EA\frac{\partial^2 \bar{u}}{\partial x^2} + ES_1\frac{\partial^2 \phi}{\partial t^2} = \rho A\frac{\partial^2 \bar{u}}{\partial x^2}, \tag{33a}$$

$$f_M + ES_1\frac{\partial^2 \bar{u}}{\partial x^2} + (EK_1 + GJ_s)\frac{\partial^2 \phi}{\partial x^2} - \underline{EK_0\frac{\partial^4 \phi}{\partial x^4}} = \rho I_p\frac{\partial^2 \phi}{\partial t^2} - \underline{\rho K_0\frac{\partial^4 \phi}{\partial t^2 \partial x^2}}, \tag{33b}$$

the natural boundary conditions at $x = 0$ and L are

$$0 = \frac{\partial^2 \phi}{\partial x^2}, \tag{34a}$$

$$F_T = EA\frac{\partial \bar{u}}{\partial x} + ES_1\frac{\partial \phi}{\partial x}, \tag{34b}$$

$$F_M = ES_1\frac{\partial \bar{u}}{\partial x} + (EK_1 + GJ_s)\frac{\partial \phi}{\partial x} - \underline{EK_0\frac{\partial^3 \phi}{\partial x^3} + \rho K_0\frac{\partial^3 \phi}{\partial t^2 \partial x}}, \tag{34c}$$

where the sectional integrals $S_1, K_0, K_1, D_{02}, J_s, I_p$ are defined as follows:

$$S_i = \iint_A \frac{\partial^i \psi}{\partial x^i}\,\mathrm{d}y\,\mathrm{d}z, \tag{35a}$$

$$K_i = \iint_A \left(\frac{\partial^i \psi}{\partial x^i}\right)^2 \mathrm{d}y\,\mathrm{d}z, \tag{35b}$$

$$D_{ij} = \iint_A \frac{\partial^i \psi}{\partial x^i}\frac{\partial^j \psi}{\partial x^j}\,\mathrm{d}y\,\mathrm{d}z, \tag{35c}$$

$$J_s = \iint_A \left(\frac{\partial \psi}{\partial y} - z\right)^2 + \left(\frac{\partial \psi}{\partial z} + y\right)^2 \mathrm{d}y\,\mathrm{d}z, \tag{35d}$$

$$I_p = \iint_A r^2\,\mathrm{d}y\,\mathrm{d}z \quad \text{where } i,j = 0,1,2,\ldots\ . \tag{35e}$$

The derivation of Eqs. (33)–(34) assumes that the modified Saint-Venant's warping function has odd symmetry, which causes many sectional integrals to vanish. For example, $S_i = 0$ when i is even, and $D_{ij} = 0$ when i and j are not both even or both odd. While we are not aware of general proofs for the odd symmetry of ψ, it holds true for a wide range of specific cross-sectional geometries such as triangles, rectangles, and ellipses [10,15,16].

Eqs. (33) and (34) are the same as the governing equations derived by Rosen [1] except for the underlined, fourth-order terms involving the sectional integral K_0. The ϕ'''' term comes from the inclusion of non-uniform torsion in Eq. (16a), and the $\ddot{\phi}''$ term comes from the mixed derivative term in Eq. (8). These terms are responsible for subtle effects on the resonance frequencies that are missing in Rosen's equations; as will be shown in Sections 3.1 and 3.3, the small magnitude of K_0 relative to I_p and $EK_1 + GJ_s$ leaves the fundamental frequencies unaffected while altering higher harmonics.

3. Pretwisted beams with rectangular cross-sections

To test how well the above equations capture the behaviour of pretwisted beams, the resonance frequencies and the corresponding mode shapes for rectangular cross-sectioned beams were found semi-analytically and compared to a FEA solution. A simple, free–free boundary condition is used so that Eqs. (34), the natural boundary conditions; and Eqs. (33), the equations of motion, are used without the forcing terms f_T, f_M or F_T, F_M. To determine the sectional integrals, a two-term approximation of the warping function for

rectangular cross-sections is used [10]

$$\psi(\eta,\zeta)=\eta\zeta-\frac{8a^2}{\pi^3}\frac{\sinh\dfrac{\pi\zeta}{a}}{\cosh\dfrac{\pi b}{2a}}\sin\frac{\pi\eta}{a}. \tag{36}$$

Eqs. (33) and (34) are then fully defined by four non-dimensional parameters: v, the Poisson's ratio; SL, the beam slenderness ratio; AR, the cross-sectional aspect ratio; and kL, the total pretwist angle.

3.1. Solving the equation of motion

Eqs. (33) and (34) are first non-dimensionalized by applying the scaling scheme introduced in Section 2.2; the governing equations can be rewritten in the following form:

$$f_{Ts}+\frac{\partial^2\bar{u}_s}{\partial x_s^2}+a_1\frac{\partial^2\phi_s}{\partial x_s^2}=\frac{\partial^2\bar{u}_s}{\partial t_s^2}, \tag{37a}$$

$$a_4 f_{Ms}+a_1\frac{\partial^2\bar{u}_s}{\partial x_s^2}+a_2\frac{\partial^2\phi_s}{\partial x_s^2}-\frac{\partial^4\phi_s}{\partial x_s^4}=a_3\frac{\partial^2\phi_s}{\partial t_s^2}-\frac{\partial^4\phi_s}{\partial t_s^2\partial x_s^2}, \tag{37b}$$

where the natural boundary conditions at $x_s=0$ and 1 are

$$\frac{\partial^2\phi_s}{\partial x_s^2}=0, \tag{38a}$$

$$\frac{\partial\bar{u}_s}{\partial x_s}+b_1\frac{\partial\phi_s}{\partial x_s}=\frac{F_T}{Lf_{T0}}, \tag{38b}$$

$$b_2\frac{\partial\bar{u}_s}{\partial x_s}+b_3\frac{\partial\phi_s}{\partial x_s}-b_4\frac{\partial^3\phi_s}{\partial x_s^3}+b_4\frac{\partial^3\phi_s}{\partial t_s^2\partial x_s}=\frac{F_M}{L^2f_{T0}}, \tag{38c}$$

and the coefficients $a_1,\ldots,a_4$ and $b_1,\ldots,b_4$ are

$$a_1=\frac{LS_1}{\sqrt{K_0A}},\quad a_2=\frac{L^2}{K_0}\left(K_1+\frac{G}{E}J_s\right),\quad a_3=\frac{L^2I_p}{K_0},\quad a_4=L^2\sqrt{\frac{A}{K_0}}\frac{f_{M0}}{f_{T0}}, \tag{39a}$$

$$b_1=\frac{S_1L}{\sqrt{K_0A}},\quad b_2=\frac{S_1}{L^2A},\quad b_3=\frac{EK_1+GJ_s}{E\sqrt{K_0A}},\quad b_4=\frac{1}{L^2}\sqrt{\frac{K_0}{A}}. \tag{39b}$$

The solutions are then assumed to be of the following form:

$$\bar{u}_s(x_s,t_s)=U\mathrm{e}^{\lambda_s x_s}\mathrm{e}^{\mathrm{i}\omega_s t_s},$$

$$\phi_s(x_s,t_s)=\Phi\mathrm{e}^{\lambda_s x_s}\mathrm{e}^{\mathrm{i}\omega_s t_s}. \tag{40}$$

Substituting Eqs. (40) into Eqs. (37) results in an amplitude ratio AP_s,

$$AP_s=\frac{\Phi}{U}=-\frac{\lambda_s^2+\omega_s^2}{2\lambda_s^2}, \tag{41}$$

and a characteristic equation of the form

$$A_1\lambda_s^6+(A_2+A_3\omega_s^2)\lambda_s^4+(A_4\omega_s^2+A_5\omega_s^4)\lambda_s^2+\omega_s^4=0, \tag{42}$$

where the coefficients $A_1, \ldots, A_5$ are combinations of coefficients $a_1, \ldots, a_4$ in Eqs. (37). The characteristic equation has six complex roots $\lambda_{s,1}, \ldots, \lambda_{s,6}$ which are functions of ω_s. The solution thus has the form

$$\bar{u}_s(x_s, t_s) = \sum_{j=1}^{6} U_j e^{\lambda_{s,j}(\omega_s)x_s} e^{i\omega_s t_s}, \tag{43a}$$

$$\phi_s(x_s, t_s) = \sum_{j=1}^{6} AP_j U_j e^{\lambda_{s,j}(\omega_s)x_s} e^{i\omega_s t_s}. \tag{43b}$$

Substituting Eqs. (43) into the six boundary conditions in Eqs. (38) results in a matrix equation

$$[BC]\mathbf{U} = 0, \tag{44}$$

where $\mathbf{U} = [U_1, \ldots, U_6]^T$ determines the mode shape and $[BC]$ is a 6×6 matrix whose entries are composed of complicated functions of ω_s. The natural frequencies $\omega_{s,n}$ are given by the solutions to the transcendental equation

$$\det([BC]) = 0, \tag{45}$$

and the corresponding mode shapes are determined from the null space of $[BC]$ after the substitution of $\omega_{s,n}$.

In the present work, the roots of Eq. (45) were found numerically using the secant method. The root-finding algorithm was set to terminate when $\det([BC]) < 10^{-8}$, and the initial root-containing intervals were obtained by plotting $\det(BC)$ and extracting the intervals where a sign change takes place. Due to the presence of exponential functions, numerical evaluation of $\det(BC)$ is highly sensitive to machine round-off errors. The problem was overcome through the use of the arbitrary precision arithmetics of *Mathematica* 5.0 (Wolfram Research Inc., Champaign, Illinois). An example of the curve of $\det([BC])$ as a function of ω_s is shown in Fig. 3.

To validate the numerical methods employed, we compare the resonance frequencies predicted by the current method with those predicted by prismatic bar theory. The non-dimensionalized torsional and axial resonance frequencies $(\omega_{s,T_0}, \omega_{s,A_0})$, according to the prismatic bar theory, are

$$\omega_{s,T_0} = n\pi\sqrt{\frac{GJ_s}{EI_p}}, \quad n = 1, 2, \ldots, \tag{46a}$$

$$\omega_{s,A_0} = m\pi, \quad m = 1, 2, \ldots, \tag{46b}$$

which are shown, respectively, in Fig. 3 as '+'s and '×'s. When the pretwist is zero, the predictions from Eqs. (33) and (34) are expected to match those of Eqs. (46); Fig. 3 shows that this is true for the axial resonance frequencies ω_{s,A_0}. While some deviation of the torsional resonance frequencies can be seen for the higher harmonics, the fundamental torsional resonance frequency shows remarkable agreement with the

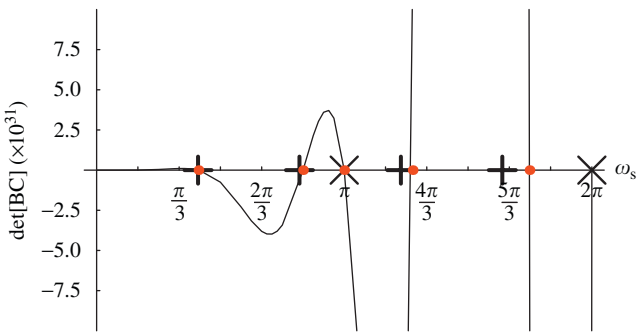

Fig. 3. Determining the natural frequencies: the plot of $\det([BC])$ as a function of ω_s at aspect ratio = 0.4, slenderness ratio = 0.1, pretwist = 0, $\nu = 0.3$. The roots found from the secant method are marked with red dots. The points corresponding to ω_{s,T_0} and ω_{s,A_0} are marked, respectively, with '+'s and '×'s (colour online).

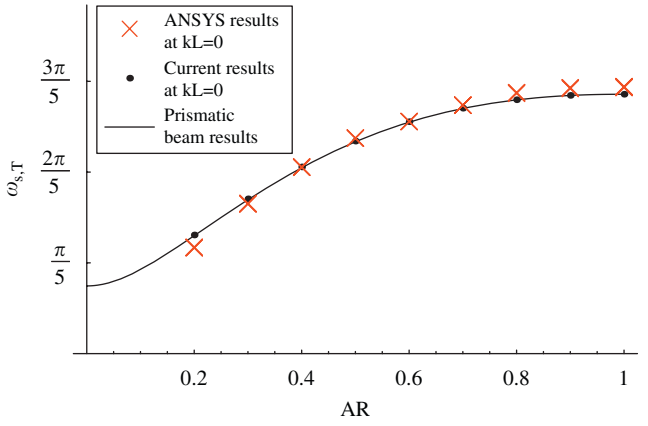

Fig. 4. A comparison between the first resonance frequency at $kL = 0$ determined by the analysis presented in this paper and the fundamental torsional resonance frequencies predicted by simple prismatic bar theory (colour online).

prismatic beam results, as illustrated in Fig. 4, where the first non-zero root of Eq. (45) is compared with the ω_{s,T_0} predicted by Eq. (46a) and FEA. This result lends credence to the method employed in solving the equations of motion.

A representative set of vibration mode shapes is shown in Fig. 5, where the mode number n denotes that the mode corresponds to the n-th non-zero solution to Eq. (45). Whether the n-th root represents an axial or torsional resonance can be inferred from its frequency and the observed mode shape. For example, the vibration mode at $n = 3$ is an axial resonance because it has no torsional motion, $\phi_s = 0$, and $\omega_{s,3} = \pi$ corresponds to the fundamental axial resonance of prismatic bars. The status of the other frequencies is more ambiguous, due to significant coupling between torsional and axial motion, however, $n = 1$ can be traced to the fundamental torsional resonance frequency of prismatic bar theory (as shown in Fig. 4), thus $n = 1$, 2, 4 and 5 are predominantly torsional modes.

We determined the variation of the fundamental torsional resonance frequency $\omega_{s,1}$ for a wide range of geometries. The pretwist kL is increased from 0 to 2 revolutions, the cross-section aspect ratio (AR $= b/a$) was varied from 0.2 to 0.9, and the beam slenderness ratios (SL $= r_c/L$) were examined at 0.1, 0.05 and 0.025. The sole relevant material property—Poisson's ratio—was fixed at 0.3, as reasoned before. The results for the fundamental torsional resonance $\omega_{s,T}$ are summarized in Section 3.3, where instead of kL, the helix angle $\alpha = \tan^{-1}(kL\mathrm{SL})$ is used to characterize the rate of pretwist (allowing the collapse of the results from the three different slenderness ratios onto the same curves).

3.2. Finite-element analysis

FEA modal of pretwisted beams was performed using ANSYS 10.0 (ANSYS Inc., Canonsburg, PA, USA). The resonance frequencies and the vibration mode shapes were determined over the same range of geometric configurations used for the analytical solutions. In order to automate the identification of the vibration modes of the FEA results—to determine whether the mode is flexural, axial or torsional—we define a modal identification parameter Λ_i adapted from [17]

$$\Lambda_i = \frac{1}{S}\oint_s \frac{\mathbf{u}\cdot\mathbf{e}_i}{|\mathbf{u}|}\,\mathrm{d}s, \tag{47}$$

where the path integral is performed along the cross-section perimeter at the beam tip, S is the path length, and i denotes the vibration mode of interest. The parameter Λ_i varies between -1 and 1, and represents a normalized average of the displacement component in the $\mathbf{e}_i$ direction, where $\mathbf{e}_\phi$ is associated with torsional vibration, and $\mathbf{e}_x$ is associated with axial vibration. In Fig. 6, the parameters Λ_ϕ and Λ_x are plotted against frequency for the first 30 modes of all geometries considered in the FEA. The path integral for Λ_i was evaluated as a discretized summation over 60 divisions (15 per edge) along the cross-section perimeter.

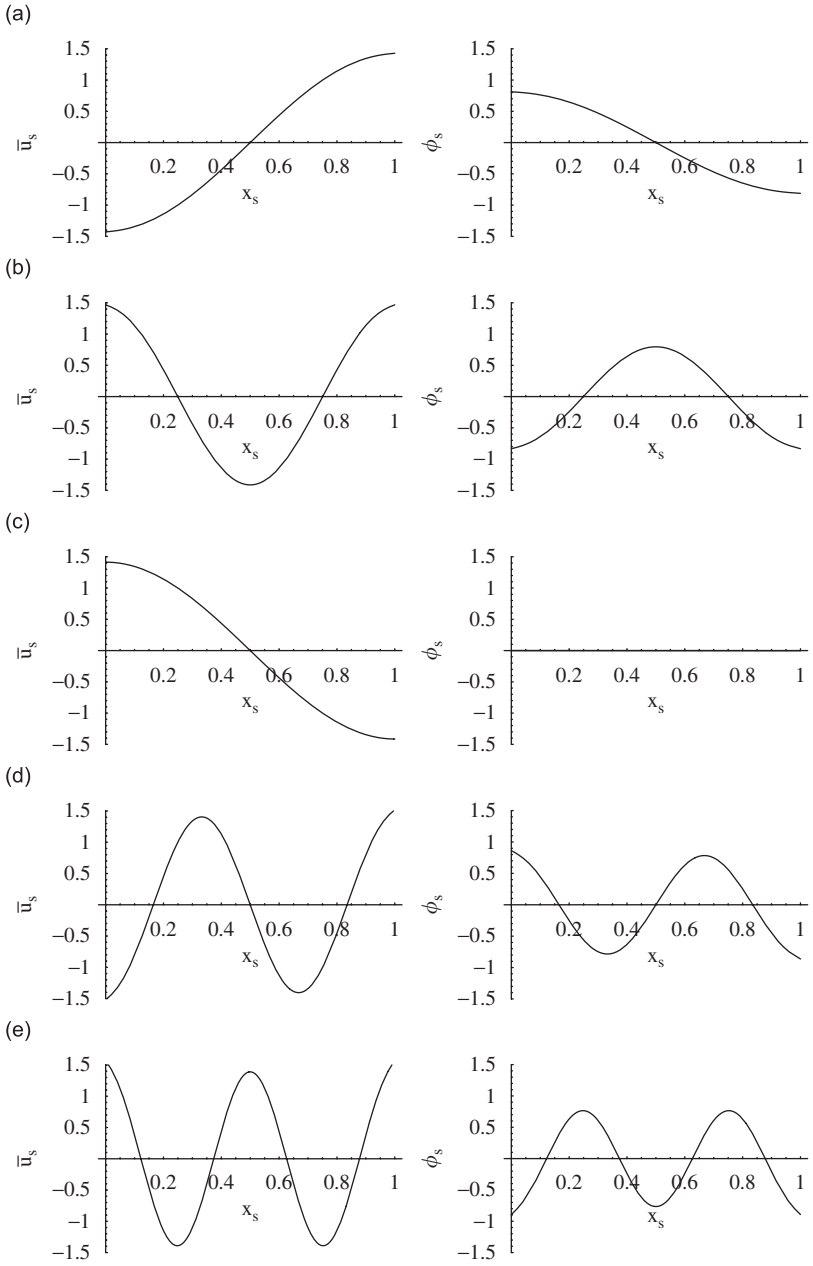

Fig. 5. The vibration mode shapes of an rectangular beam with aspect ratio = 0.4, slenderness ratio = 0.1, pretwist = 0.1 revolution (helix angle = 3.6°): (a) mode number $n = 1$, $\omega_{s,1} = 0.41\pi$ (torsional resonance), (b) mode number $n = 2$, $\omega_{s,2} = 0.83\pi$ (torsional resonance), (c) mode number $n = 3$, $\omega_{s,3} = 1.0\pi$ (axial resonance), (d) mode number $n = 4$, $\omega_{s,4} = 1.3\pi$ (torsional resonance) and (e) mode number $n = 5$, $\omega_{s,5} = 1.7\pi$ (torsional resonance).

It shows that Λ_ϕ and Λ_x work well as identification parameters for the presence of torsional and axial components in a vibration mode. At low frequencies, the modes are quite distinct and a simple mode classification rule can be used:

- Torsional modes: $|\Lambda_\phi| \geqslant 0.9$, represented by black dots in Fig. 6.
- Axial modes: $|\Lambda_x| \geqslant 0.9$, represented by red boxes in Fig. 6.

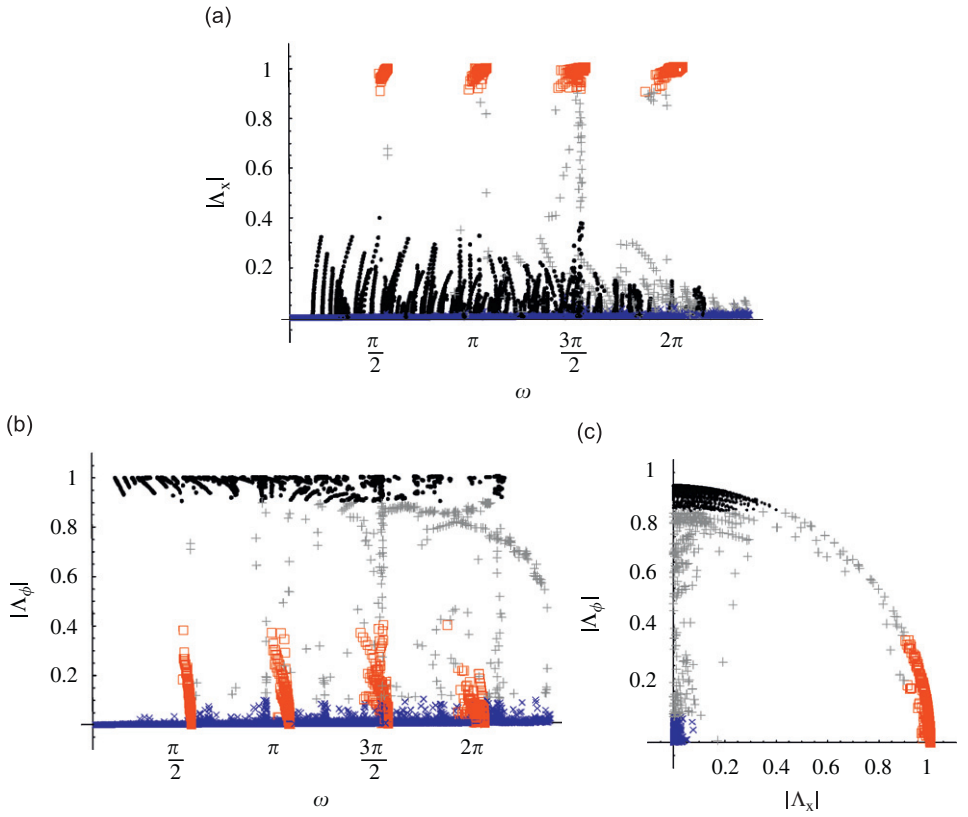

Fig. 6. The modal identification parameters Λ_ϕ and Λ_x vs. non-dimensionalized frequency for the first 30 modes of all geometries considered by FEA. The black dots, red squares, blue x's, and grey plus signs are correspondingly, those points with $|\Lambda_\phi| \geqslant 0.9$ (torsional modes), $|\Lambda_x| \geqslant 0.9$ (axial modes), $|\Lambda_{\phi,x}| \leqslant 0.1$ (flexural modes) and $0.1 < |\Lambda_{\phi,x}| < 0.9$ (mixed modes) (colour online).

- Flexural modes: $|\Lambda_\phi| \leqslant 0.1$ and $|\Lambda_x| \leqslant 0.1$, represented by blue '×'s in Fig. 6.
- Mixed modes: $0.1 < |\Lambda_\phi| < 0.9$ and $0.1 < |\Lambda_x| < 0.9$, represented by grey '+'s in Fig. 6.

The first axial and torsional mode for each geometry, as classified by the above scheme, are, respectively, taken as the fundamental axial and torsional resonance $\omega_{s,A}$ and $\omega_{s,T}$. The results are summarized in Fig. 7.

At higher harmonics, a significant amount of coupling is present for various geometries. Note especially the series of resonance modes that lie along the unit circle in Fig. 6(c) and form vertical lines at $\omega_s \simeq 3\pi/2$ in Fig. 6(a) and (b). These modes belong to geometries with SL = 0.1 and AR $\simeq$ 1, in other words, thick square beams. Many points in this series are close to the maximum coupling point of $\Lambda_\phi = \Lambda_x = 1/\sqrt{2}$.

3.3. Comparison of the theoretical predictions with the FEA results

3.3.1. Rosen's equations

The equations of motion derived in the present work contain extra fourth-order terms compared to Rosen's equations of motion [1]. Table 3 shows, however, that the non-dimensionalized coefficients of the second-order terms are 2–4 orders of magnitude greater than the fourth-order terms (see Eqs. (37)). Hence the differences between Eqs. (33) and Rosen's equations in the prediction of the fundamental resonance frequencies ($\omega_{s,T}, \omega_{s,A}$) are negligible. Their frequency plots both appear identical to the solid lines in Fig. 7: both analytical methods predict a rise in $\omega_{s,T}$ and $\omega_{s,A}$ as the rate of pretwist α is increased, both predict that $\omega_{s,T}$ will increase as the cross-section approaches a square (AR = 1), and both predict that the effect of pretwist is amplified as the cross-section become thinner.

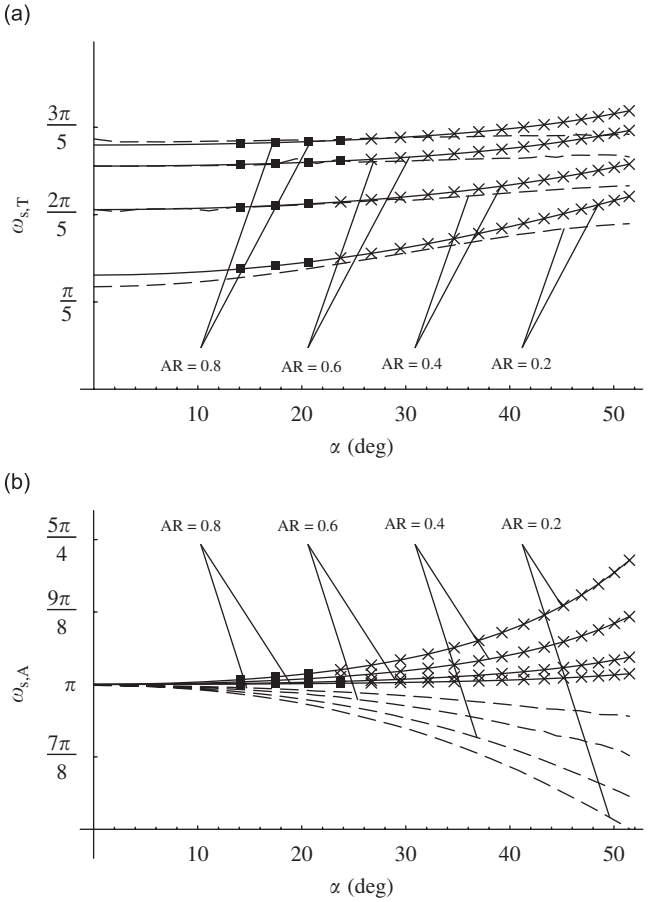

Fig. 7. Fundamental resonance frequencies for pretwisted rectangular cross-sectioned beams as pretwist (helix angle α), and aspect ratio ($AR = b/a$) are varied: (a) torsional mode $\omega_{s,T}$, and (b) axial mode $\omega_{s,A}$. The solid and the dashed lines are, respectively, results from the present theory and the FEA results. The boxes and crosses mark the points that, respectively, lie outside the $\varepsilon = 0.05$ and the $\varepsilon = 0.1$ criteria.

Table 3
Coefficients of the second-order terms in the non-dimensionalized equations of motion Eqs. (37) when slenderness ratio SL = 0.1

Aspect ratio AR	Helix angle α	Torsional stiffness a_2	Rotational inertia a_3
0.2	0	615	9111
	51°	6316	9111
0.9	0	6100	18848
	51°	10303	18848

It should be pointed out that the above result should not be interpretations as a justification to neglect ϕ'' and $\dot{\phi}'$ in the derivation of the equation of motion. As shown earlier ϕ_s'' and $\dot{\phi}_s'$ are of similar or greater magnitude than commonly retained terms such as ϕ_s' and $\dot{\phi}_s$:

$$\phi_s(x_s) \sim \Phi \cos(\lambda_s x_s) e^{i\omega_s t_s} \quad \text{implies } |\phi_s''| \sim \lambda_s |\phi_s'| \quad \text{and} \quad |\dot{\phi}_s'| \sim \lambda_s |\dot{\phi}_s|. \tag{48}$$

In order to neglect the fourth-order terms that arise from the inclusion of ϕ'' and $\dot{\phi}'$ in the derivation, the magnitude of their influence coefficients in the final equations of motion need to be considered, which cannot

be determined if ϕ'' and $\dot{\phi}'$ are neglected *a priori*. Additionally, the influence of the fourth-order terms becomes noticeable at higher harmonics since $\lambda_s \gg 1$, as Fig. 3 indicates.

3.3.2. *Differences and similarities*

One of the chief contributions of this study is the derivation of an objective and measurable criteria for checking the validity of the assumption that the warping function of pretwisted beams are locally similar to that of a prismatic beam. In this section, the limitations of the simplified warping function are revealed by comparing FEA results with Rosen's and our analytical predictions (which are based on the warping function of prismatic beams).

The analytical predictions of the fundamental torsional resonance frequencies $\omega_{s,T}$ show a good agreement with FEA results when the helix angle is below 30° and the aspect ratio is above 0.2; however, at high rates of pretwist and low aspect ratios, the analytical solutions significantly overpredict $\omega_{s,T}$.

It may be seen in Fig. 7(a) that many solutions lying in the invalid region according to our criteria (marked with crosses) in fact match the FEA results quite well. This apparent contradiction with the scaling analysis may lead one to question the criteria used to judge the validity of the solution. However, when the corresponding points in Fig. 7(b) are considered, it can be seen that the criteria were in fact picking up geometries for which the predicted axial resonance frequencies deviated significantly from the FEA results.

The poor prediction of the axial resonance frequencies by warping function based pretwisted beam theories has existed in the literature for a long time without adequate explanation [1,8]. Our warping function criteria finally show that this discrepancy may be traced to use of the modified prismatic warping function where it is no longer valid. If the simplified prismatic warping function is invalid, Eqs. (24) and (25) suggest that the warping function is deformation dependent and variable along the beam's axis. Thus for beams with sufficient pretwist, the application of the modified prismatic warping function effectively "clamps" the cross-section to warp in the manner prescribed by Eqs. (31), resulting in higher stiffness and causing the simple theory to overpredict the resonance frequencies.

3.3.3. *Warping function of rectangular cross-sections*

A source of error in this study is the warping function used for rectangular cross-sections. The solution to Eq. (28b) for rectangular cross-sections with width a and height b is an infinite series [10]

$$\psi(\eta,\zeta) = \eta\zeta - \frac{8a^2}{\pi^3}\sum_{n=0}^{\infty}\frac{(-1)^n}{(2n+1)^3}\frac{\sinh k_n\zeta}{\cosh(k_n b/2)}\sin k_n\eta,$$

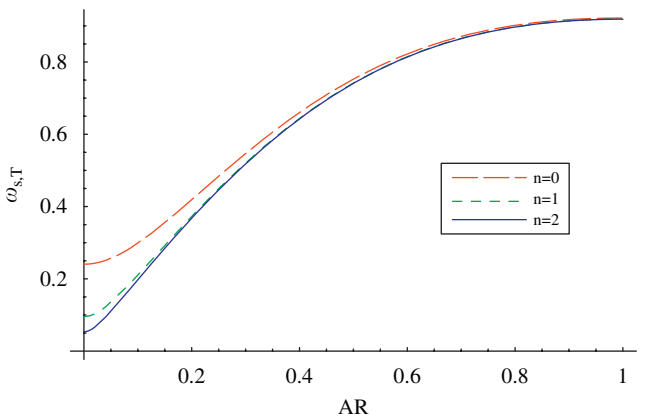

Fig. 8. The effect of neglecting higher-order terms of the warping function for rectangular cross-sections. The variation of the fundamental torsional resonance frequency $\omega_{s,T}$ predicted by the prismatic bar theory is plotted against AR when the warping function is evaluated to the n-th term.

where

$$k_n = \frac{(2n+1)\pi}{a}. \tag{49}$$

Due to the complex sectional integrals involved in Eqs. (33)–(35), the warping function was only evaluated to the $n = 0$ term in Section 3.1. The effect of neglecting the higher-order terms at zero pretwist can be seen in Fig. 8, where $\omega_{s,T}$ predicted by prismatic beam theory is plotted against AR as successively more terms are included in ψ. The torsional resonance frequency should approach zero as AR $\to 0$. However, due to the series approximation of ψ, an erroneous finite $\omega_{s,T}$ is predicted. As more terms are included in ψ, the more accurate the $\omega_{s,T}$ predictions become at low AR.

4. Conclusions

The prismatic beam warping function is commonly used in theories for pretwisted beams without an understanding of its limitations. Through scaling analysis of the equations governing the warping function of pretwisted beams—which we derive carefully from Hamilton's principle—a set of criteria for checking the validity of the simplifying assumption is obtained. Comparison of warping function-based analytical solutions with FEA results show that the misuse of the prismatic warping function is responsible for the poor prediction of the axial resonance frequencies in the literature [1,8].

Inconsistencies in Rosen's equations of motion for axial–torsional coupling in pretwisted beams are also corrected; the inclusion of ϕ'' and $\dot{\phi}$ in the derivation leads to the addition of fourth-order terms in the equations of motion. The small size of the coefficients of the fourth-order terms means that the fundamental resonance frequencies predicted by the fourth-order equation are essentially the same as Rosen's theory, however, the fourth-order terms becomes significant for higher harmonics.

Appendix A. Hamilton's principle and the resulting Euler–Lagrange equation

To apply Hamilton's principle, the strain energy equation (20), the kinetic energy equation (22), and the work done by external loads equation (23) are substituted into Eq. (4), resulting in an equation of the form

$$\delta\left(\int_{t_1}^{t_2}\iiint_V F(x,y,z,t,\bar{u},\phi,\psi)\,\mathrm{d}V\,\mathrm{d}t\right) = 0, \tag{A.1}$$

where

$$\begin{aligned} F(x,y,z,t,\bar{u},\phi,\psi) = {} & \frac{1}{2}E(\bar{\varepsilon}_{xx}^2 + (\theta'\psi)^2 + (\theta\psi')^2 + 2\bar{\varepsilon}_{xx}\theta'\psi + 2\bar{\varepsilon}_{xx}\theta\psi' + 2\theta'\theta\psi'\psi) \\ & + \frac{1}{2}G\theta^2\left[\left(\frac{\partial\psi}{\partial y} - z\right)^2 + \left(\frac{\partial\psi}{\partial z} + y\right)^2\right] + \frac{1}{2}\rho[\dot{\bar{u}}^2 + 2\dot{\bar{u}}\dot{\theta}\psi + \dot{\theta}^2\psi^2 + r^2\dot{\phi}^2] \\ & + \frac{\mathrm{d}F_T}{\mathrm{d}A}\bar{\varepsilon}_{xx} + \frac{\mathrm{d}F_M}{\mathrm{d}A}\theta + \frac{\mathrm{d}f_T}{\mathrm{d}A}\bar{u} + \frac{\mathrm{d}f_M}{\mathrm{d}A}\phi. \end{aligned} \tag{A.2}$$

The Euler–Lagrange equation resulting from Eq. (A.1) is

$$\int_{t_1}^{t_2}\iiint_V \eta_{\bar{u}}\left[\frac{\partial F}{\partial\bar{u}} - \frac{\partial}{\partial x}\frac{\partial F}{\partial\bar{\varepsilon}_{xx}} - \frac{\partial}{\partial t}\frac{\partial F}{\partial\dot{\bar{u}}}\right]\mathrm{d}V\,\mathrm{d}t + \int_{t_1}^{t_2}\oiint \eta_{\bar{u}}\frac{\partial F}{\partial\bar{\varepsilon}_{xx}}a_{nx}\,\mathrm{d}A\,\mathrm{d}t + \iiint_V \eta_{\bar{u}}\frac{\partial F}{\partial\dot{\bar{u}}}\bigg|_{t_1}^{t_2}\mathrm{d}V = 0, \tag{A.3a}$$

$$\begin{aligned} & \int_{t_1}^{t_2}\iiint_V \eta_\phi\left[\frac{\partial F}{\partial\phi} - \frac{\partial}{\partial x}\frac{\partial F}{\partial\theta} - \frac{\partial}{\partial t}\frac{\partial F}{\partial\dot{\phi}} + \frac{\partial^2}{\partial x^2}\frac{\partial F}{\partial\theta'} + \frac{\partial^2}{\partial x\partial t}\frac{\partial F}{\partial\dot{\theta}}\right]\mathrm{d}V\,\mathrm{d}t \\ & + \int_{t_1}^{t_2}\oiint\left(\eta_\phi\left[\frac{\partial F}{\partial\theta} - \frac{\partial}{\partial x}\frac{\partial F}{\partial\theta'} - \frac{\partial}{\partial t}\frac{\partial F}{\partial\dot{\theta}}\right]a_{nx} + \eta'_\phi\frac{\partial F}{\partial\theta'}a_{nx}\right)\mathrm{d}A\,\mathrm{d}t + \iiint_V \eta_\phi\frac{\partial F}{\partial\dot{\theta}}\bigg|_{t_1}^{t_2} + \eta'_\phi\frac{\partial F}{\partial\dot{\theta}}\bigg|_{t_1}^{t_2}\mathrm{d}V = 0, \end{aligned} \tag{A.3b}$$

$$\int_{t_1}^{t_2}\iiint_V \eta_\psi\left[\frac{\partial F}{\partial \psi}-\frac{\partial}{\partial x}\frac{\partial F}{\partial \psi'}-\frac{\partial}{\partial y}\frac{\partial F}{\partial \psi_{,y}}+\frac{\partial}{\partial z}\frac{\partial F}{\partial \psi_{,z}}\right]\mathrm{d}V\,\mathrm{d}t+\int_{t_1}^{t_2}\oiint \eta_\psi\left(\frac{\partial F}{\partial \psi'}a_{nx}+\frac{\partial F}{\partial \psi_{,y}}a_{ny}+\frac{\partial F}{\partial \psi_{,z}}a_{nz}\right)\mathrm{d}A\,\mathrm{d}t=0, \tag{A.3c}$$

where $\eta_{\bar{u}},\eta_\phi,\eta_\psi$ represents three independent arbitrary functions and the variational derivatives of F are

$$\frac{\partial F}{\partial \bar{u}}=\frac{\mathrm{d}f_T}{\mathrm{d}A},\quad \frac{\partial F}{\partial \dot{\bar{u}}}=\rho(\dot{\bar{u}}+\dot{\theta}\psi),\quad \frac{\partial F}{\partial \bar{\varepsilon}_{xx}}=-E(\bar{\varepsilon}_{xx}+\theta'\psi+\theta\psi')+\frac{\mathrm{d}F_T}{\mathrm{d}A},$$

$$\frac{\partial F}{\partial \phi}=\frac{\mathrm{d}f_M}{\mathrm{d}A},\quad \frac{\partial F}{\partial \dot{\phi}}=\rho r^2\dot{\phi},\quad \frac{\partial F}{\partial \theta'}=-E(\theta'\psi^2+\bar{\varepsilon}_{xx}\psi+\theta\psi\psi'),$$

$$\frac{\partial F}{\partial \theta}=-E(\theta\psi'^2+\bar{\varepsilon}_{xx}\psi'+\theta'\psi\psi')-G\theta[(\psi_{,y}-z)^2+(\psi_{,y}+z)^2]+\frac{\mathrm{d}F_M}{\mathrm{d}A},$$

$$\frac{\partial F}{\partial \dot{\theta}}=\rho(\dot{\bar{u}}\psi+\dot{\theta}\psi^2),\quad \frac{\partial F}{\partial \psi_{,y}}=-G\theta^2(\psi_{,y}-z),\quad \frac{\partial F}{\partial \psi_{,z}}=-G\theta^2(\psi_{,z}+y),$$

$$\frac{\partial F}{\partial \psi}=\rho(\dot{\theta}\dot{\bar{u}}+\dot{\theta}^2\psi)-E(\theta'^2\psi+\bar{\varepsilon}_{xx}\theta'+\theta\theta'\psi'),$$

$$\frac{\partial F}{\partial \psi'}=-E(\theta^2\psi'+\bar{\varepsilon}_{xx}\theta+\theta\theta'\psi). \tag{A.4}$$

Substituting Eq. (A.4) into the Euler–Lagrange equation (A.3) gives the equations of motion, the boundary conditions, and the initial conditions.

The initial conditions can be determined from the following equations:

$$\eta_{\bar{u}}\frac{\partial F}{\partial \dot{\bar{u}}}\bigg|_{t_1}^{t_2}=0,\quad \eta_\phi\frac{\partial F}{\partial \dot{\phi}}\bigg|_{t_1}^{t_2}=0,\quad \eta'_\phi\frac{\partial F}{\partial \dot{\theta}}\bigg|_{t_1}^{t_2}=0, \tag{A.5}$$

which implies that the following initial conditions needs to be specified: $\bar{u}(x,0)$, $\phi(x,0)$, $\theta(x,0)$, $\dot{\bar{u}}(x,0)+\dot{\theta}(x,0)\psi$, and $\dot{\phi}(x,0)$.

Appendix B. Normal vectors on the surface of pretwisted beams

The surface of a constant cross-section pretwisted beam can be described by the following position vector (see Fig. B1):

$$\mathbf{r}(x,s)=x\mathbf{e}_x+\boldsymbol{\Gamma}(s), \tag{B.1}$$

where $\boldsymbol{\Gamma}(s)$ traces the perimeter of the cross-sectional geometry with the path variable s

$$\begin{aligned}\boldsymbol{\Gamma}(s)&=\eta(s)\mathbf{e}_\eta+\zeta(s)\mathbf{e}_\zeta\\&=(\eta(s)\cos kx-\zeta(s)\sin kx)\mathbf{e}_y+(\eta(s)\sin kx+\zeta(s)\cos kx)\mathbf{e}_z.\end{aligned} \tag{B.2}$$

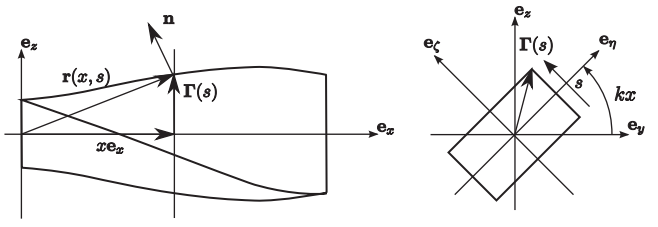

Fig. B1. Two parameter (x,s) description of the surface of a pretwisted beam.

Normal vectors can be obtained from the cross product of two non-parallel tangent vectors to the surface of the pretwisted beam, thus

$$\mathbf{n} = \frac{\partial \mathbf{r}}{\partial s} \times \frac{\partial \mathbf{r}}{\partial x}. \tag{B.3}$$

Expressing Eq. (B.1) in array form,

$$\mathbf{r}(x,s) = \begin{bmatrix} x \\ \eta \cos kx - \zeta \sin kx \\ \eta \sin kx + \zeta \cos kx \end{bmatrix}, \tag{B.4}$$

the tangent vectors are obtained as

$$\frac{\partial \mathbf{r}}{\partial s}(x,s) = \begin{bmatrix} 0 \\ \eta' \cos kx - \zeta' \sin kx \\ \eta' \sin kx + \zeta' \cos kx \end{bmatrix} \quad \text{and} \quad \frac{\partial \mathbf{r}}{\partial x}(x,s) = \begin{bmatrix} 1 \\ -k(\eta \sin kx + \zeta \cos kx) \\ k(\eta \cos kx - \zeta \sin kx) \end{bmatrix}. \tag{B.5}$$

Substituting Eq. (B.5) into Eq. (B.3) yields

$$\mathbf{n} = \begin{bmatrix} k(\eta\eta' + \zeta\zeta') \\ \eta' \sin kx + \zeta' \cos kx \\ -\eta' \cos kx + \zeta' \sin kx \end{bmatrix}, \tag{B.6}$$

which can then be used to determine the components of the unit normal vector $\hat{\mathbf{n}}$:

$$\hat{\mathbf{n}} = \frac{\mathbf{n}}{|\mathbf{n}|} = [a_{nx}, a_{ny}, a_{nz}]^{\mathrm{T}}. \tag{B.7}$$

From Eq. (B.6), the component of the unit normal vector in the radial direction a_{nr} is

$$a_{nr} = \sqrt{a_{ny}^2 + a_{nz}^2} = \frac{1}{|\mathbf{n}|}\sqrt{(\eta')^2 + (\zeta')^2}, \tag{B.8}$$

which can be used to determine the following ratios, which are needed for comparing the magnitude of the NDCs in Table 2,

$$\frac{a_{nx}}{a_{nr}} = \frac{k(\eta\eta' + \zeta\zeta')}{\sqrt{(\eta')^2 + (\zeta')^2}}, \tag{B.9a}$$

$$\frac{a_{ny}}{a_{nr}} = \frac{\eta' \sin kx + \zeta' \cos kx}{\sqrt{(\eta')^2 + (\zeta')^2}}, \tag{B.9b}$$

$$\frac{a_{nz}}{a_{nr}} = \frac{-\eta' \cos kx + \zeta' \sin kx}{\sqrt{(\eta')^2 + (\zeta')^2}}. \tag{B.9c}$$

B.1. Elliptical cross-section

For a beam with an elliptical cross-section

$$\eta(s) = a\cos(s), \quad \eta'(s) = -a\sin(s), \tag{B.10}$$

$$\zeta(s) = b\sin(s), \quad \zeta'(s) = b\cos(s). \tag{B.11}$$

Substituting Eq. (B.10) into Eq. (B.9a) yields

$$\frac{a_{nx}}{a_{nr}} = \frac{k(b^2 - a^2)\cos(s)\sin(s)}{\sqrt{a^2\sin^2(s) + b^2\cos^2(s)}}, \tag{B.12}$$

$$\frac{a_{ny}}{a_{nr}} = \frac{-a\sin^2(s) + b\cos^2(s)}{\sqrt{a^2\sin^2(s) + b^2\cos^2(s)}}, \tag{B.13}$$

$$\frac{a_{ny}}{a_{nr}} = \frac{-a\sin(s)\cos(s) + b\cos(s)\sin(s)}{\sqrt{a^2\sin^2(s) + b^2\cos^2(s)}}. \tag{B.14}$$

The extreme values of a_{nx}/a_{nr} are determined by solving for the stationary points of Eq. (B.12)

$$\frac{\mathrm{d}}{\mathrm{d}s}\left(\frac{a_{nx}}{a_{nr}}\right) = \frac{(b^2 - a^2)k(b\cos^4(s) - a^2\sin^4(s))}{\sqrt{b^2\cos^2(s) + a^2\sin^2(s)}} = 0, \tag{B.15}$$

which has the solution

$$s = \tan^{-1}(\sqrt{b/a}) = \tan^{-1}(\sqrt{\mathrm{AR}}).$$

Substituting Eq. (B.16) back into Eq. (B.12) gives the extreme values of a_{nx}/a_{nr} for a beam with elliptical cross-section

$$\left(\frac{a_{nx}}{a_{nr}}\right)_{\text{extreme}} = k(b - a) = kL \times \mathrm{SL}(\mathrm{AR} - 1). \tag{B.16}$$

B.2. Rectangular cross-section

For a beam with a rectangular cross-section of width a and height b, the boundary path can be parameterized as

$$(\eta(s), \zeta(s)) = \begin{cases} (-(a/2)(-1 + 2s), b/2), & s \in (0, 1), \\ (-a/2, (b/2)(3 - 2s)), & s \in (1, 2), \\ ((a/2)(-5 + 2s), -b/2), & s \in (2, 3), \\ (a/2, -(b/2)(7 - 2s)), & s \in (3, 4), \end{cases} \tag{B.17}$$

where the derivatives are

$$(\eta'(s), \zeta'(s)) = \begin{cases} (-a, 0), & s \in (0, 1), \\ (0, -b), & s \in (1, 2), \\ (a, 0), & s \in (2, 3), \\ (0, b), & s \in (3, 4). \end{cases} \tag{B.18}$$

Substituting Eq. (B.17) into Eq. (B.9a) yields

$$\frac{a_{nx}}{a_{nr}} = \begin{cases} -k(a/2)(1 - 2s), & s \in (0, 1), \\ -k(b/2)(3 - 2s), & s \in (1, 2), \\ -k(a/2)(5 - 2s), & s \in (2, 3), \\ -k(b/2)(7 - 2s), & s \in (3, 4). \end{cases} \tag{B.19}$$

It is clear from Eq. (B.19) that the extreme values of a_{nx}/a_{nr} occurs at the corners of the cross-sections. Since $b \leqslant a$, the maximum tilt ratio for a rectangular cross-section is

$$\frac{a_{nx}}{a_{nr}} = \frac{k \times a}{2} = \frac{k \times r_c}{\sqrt{1 + \mathrm{AR}^2}} = \frac{kL \times \mathrm{SL}}{\sqrt{1 + \mathrm{AR}^2}}. \tag{B.20}$$

References

[1] A. Rosen, Structural and dynamic behaviour of pretwisted rods and beams, *Applied Mechanics Review* 44 (12) (1991) 483–515 (part 1).

[2] D. Wajchman, K.-C. Liu, J. Friend, L. Yeo, An ultrasonic piezoelectric motor utilising a non-circular cross sectioned twisted beam, *IEEE Transactions on Ultrasonics, Ferroelectrics, and Frequency Control* 55 (4) (2008) 832–840.

[3] C. Chu, The effect of initial twist on the torsional rigidity of thin prismatical bars and tubular members, *Proceedings of the First US National Congress of Applied Mechanics*, 1951, pp. 265–269.

[4] A. Rosen, The effect of initial twist on the torsional rigidity of beams—another point of view, *Journal of Applied Mechanics* 47 (1980) 389–392.

[5] A. Rosen, Theoretical and experimental investigation of the nonlinear torsion and extension of initially twisted bars, *Journal of Applied Mechanics* 50 (1983) 321–326.

[6] A.H. Hodges, Torsion of pretwisted beams due to axial loading, *Journal of Applied Mechanics* 47 (1980) 393–397.

[7] S. Krenk, A linear theory for pretwisted elastic beams, *Journal of Applied Mechanics* 50 (1983) 137–142.

[8] T. Tsuiji, Free vibrations of thin-walled pretwisted beams, *Bulletin of JSME* 28 (239) (1985) 894–898.

[9] X.S. Xu, W.X. Zhong, H.W. Zhang, The Saint-Venant problem and principle in elasticity, *International Journal of Solids and Structures* 34 (22) (1997) 2815–2827.

[10] I.S. Sokolnikoff, *Mathematical Theory of Elasticity*, McGraw-Hill Book Company, H 531.38 S683M2, 1956.

[11] S. Krenk, The torsion-extension coupling in pretwisted elastic beams, *International Journal of Solids and Structures* 19 (1) (1983) 67–72.

[12] G. Curti, A. Risitano, Coupled free, torsional and axial vibration of pre-twisted bars, *Meccanica* (1979) 157–162.

[13] J.B. Kosmatka, Extension-bend-twist coupling behaviour of nonhomogeneous anisotropic beams with initial twist, *AIAA Journal* 30 (2) (1992) 519–527.

[14] J. Li, H. Hua, R. Shen, X. Jin, Stochastic vibration of axially loaded monosymmetric Timoshenko thin-walled beam, *Journal of Sound and Vibration* 274 (3–5) (2004) 915–938.

[15] Y.-C. Fung, *Foundations of Solid Mechanics*, Prentice-Hall, Englewood Cliffs, NJ, 1965.

[16] I.H. Shames, C.L. Dym, *Solid Mechanics: A variational Approach*, McGraw-Hill, New York, 1973.

[17] J. Friend, K. Nakamura, S. Ueha, A torsional transducer through in-plane shearing of paired planar piezoelectric elements, *IEEE Transactions on Ultrasonics, Ferroelectrics, and Frequency Control* 51 (7) (2004) 871–878.